JOURNAL OF PROPULSION AND POWER
Vol. 10, No. 6, Nov.–Dec. 1994

# Modeling of Supersonic Turbulent Combustion Using Assumed Probability Density Functions

R. A. Baurle,* G. A. Alexopoulos,* and H. A. Hassan†
*North Carolina State University, Raleigh, North Carolina 27695*

**Recent calculations of turbulent supersonic reacting shear flows using an assumed multivariate $\beta$ probability density function (PDF) resulted in reduced production rates and a delay in the onset of combustion. This result is not consistent with available measurements. Earlier work was based on a one-equation turbulence model that required a specification of the length scale, PDFs that did not yield Favre-averaged quantities, and the gradient diffusion assumption. The present work incorporates a two-equation turbulence model based on a $k$-$\omega$ formulation, a PDF that yields Favre averages, and relaxes the gradient diffusion assumption. Results suggest that the form of the assumed multivariate PDF and the gradient diffusion assumption are the main causes of the discrepancy.**

## Nomenclature

| | | |
|---|---|---|
| $D$ | = | molecular diffusion coefficient |
| $D_t$ | = | turbulent diffusion coefficient |
| $k$ | = | turbulent kinetic energy |
| $k_f$ | = | forward reaction rate |
| $l$ | = | width of the mixing layer |
| $ns$ | = | number of chemical species |
| $P$ | = | pressure |
| $\mathcal{P}$ | = | probability density function |
| $T$ | = | temperature |
| $t$ | = | time |
| $u_j$ | = | velocity |
| $\dot{w}_k$ | = | species production rates |
| $X_k$ | = | species mole fractions |
| $x_j$ | = | spatial coordinates |
| $Y_k$ | = | species mass fractions |
| $\alpha$, $\beta_k$, $\beta_k^*$ | = | multivariate beta PDF parameters |
| $\Gamma$ | = | gamma function |
| $\delta$ | = | Dirac delta function |
| $\delta_{ij}$ | = | Kronecker delta |
| $\rho$ | = | density |
| $\sigma_Y$ | = | species mass fraction variance sum |
| $\sigma_\rho$ | = | species density variance sum |
| $\tau$ | = | turbulent time scale |
| $\omega$ | = | turbulent frequency |

*Subscripts*

| | | |
|---|---|---|
| $i, j, n$ | = | spatial coordinates |
| $k$ | = | species number |
| $t$ | = | turbulent quantity |

*Superscripts*

| | | |
|---|---|---|
| $\bar{}$ | = | time-averaged quantity |
| $'$ | = | fluctuating component |
| $\tilde{}$ | = | Favre-averaged quantity |
| $''$ | = | Favre fluctuating component |

Presented as Papers 93-2197 and 93-2198 at the AIAA/SAE/ASME/ASEE 29th Joint Propulsion Conference and Exhibit, Monterey, CA, June 28–30, 1993; received Aug. 27, 1993; revision received Jan. 7, 1994; accepted for publication Feb. 24, 1994. 

*Research Assistant, Mechanical and Aerospace Engineering. Student Member AIAA.

†Professor, Mechanical and Aerospace Engineering. Associate Fellow AIAA.

## Introduction

INTEREST in hypersonic air breathing propulsion has resulted in an increased research effort in the area of high-speed combustion. Due to the short residence times of these flows, the amount of turbulent mixing and the corresponding extent of combustion that can be expected will strongly effect the design considerations of such a propulsion device. Thus, a fundamental understanding of turbulence-chemistry interactions, and appropriate methods for modeling these interactions, will be a necessity.

The focus of this work is on the use of assumed probability density function (PDF) approaches to model the effects of species composition fluctuations on the chemical production rates. A first step in this direction was taken by Girimaji,[1] who proposed using a multivariate $\beta$ PDF to account for mass fraction fluctuations on the production rates. In this work, the model was shown to mimic the observed PDF from direct numerical simulation (DNS) scalar mixing data over all stages of the mixing process when only two species were considered. Unfortunately, no assessment of the model was made for larger numbers of species due to a lack of multiple scalar mixing data.

Narayan and Girimaji[2] later applied the model to simple two-dimensional reacting free shear flows and found the results from the model to have little effect on the mean flow variables. The reason for this was traced back to the chemical source term

$$\overline{Y_k'' \dot{w}_k} \tag{1}$$

that appears in the transport equation for the species mass fraction variance sum that is needed to define the PDF. This term was found to be a strong dissipative quantity in the regions where combustion was taking place. Thus, the average species production rates computed by the model were not much different from the "laminar" values.

Later, Baurle et al.[3] applied the model to an axisymmetric reacting free shear flow and comparisons were made with the experimental measurements of Cheng et al.[4] In this experiment, rms values of the fluctuating composition were measured in addition to the mean quantities allowing direct comparisons between predictions from the PDF model and experiment. This work also showed the term $\overline{Y_k'' \dot{w}_k}$ to dissipate virtually all of the species variance sum in the presence of combustion. This trend was not consistent with the experimental measurements.

Examination of the results of Ref. 3 suggests that the observed discrepancy may be a result of three different as-

sumptions. Reference 3 employed a one-equation turbulence model. Since the problem examined had two distinct shear layers, it was thought that the specification of a length scale needed for the implementation of the one-equation model may be one of the possible causes. To remedy this situation, a $k$-$\omega$ turbulence model is employed.

Another possible cause may lie in the averaging procedures in hybrid Reynolds-averaged/PDF codes. When computing compressible turbulent flowfields, Favre (or mass weighted) averaging is usually employed to reduce the number of unclosed terms in the Reynolds-averaged Navier-Stokes equations. However, this form of averaging does not help in evaluating the mean species production rates due to the high degree of nonlinearity of these terms. Because of this, the effects of fluctuations on these terms are often carried out using assumed PDF approaches that typically yield conventional time-averaged quantities. These are related to the Favre-averaged mass fractions through the relation

$$\tilde{Y}_k = \bar{Y}_k + (\overline{\rho' Y_k'}/\bar{\rho}) \tag{2}$$

where $Y_k$ is the mass fraction of species "$k$," and $\rho$ is the total density of the mixture. However, since there is no accepted procedure for modeling $\overline{\rho' Y_k'}$, $\bar{Y}_k$ is usually set equal to $\tilde{Y}_k$ and the difference between the two averages is ignored. For the assumed PDF developed by Girimaji, the model yields time-averaged mass fractions. The present work remedies this situation by expressing the PDF in terms of the species densities rather than the species mass fractions.

A third possible cause for the discrepancies with experiment lies in the modeling of $(Y_k'' u_j'')$, which appears in the production term of the species variance sum equation. Traditionally, this term is modeled with a gradient diffusion type approximation, i.e.,

$$\widetilde{Y_k'' u_j''} = -D_t \frac{\partial \tilde{Y}_k}{\partial x_j} \tag{3}$$

However, upon examination of the evolution equation governing $\widetilde{Y_k'' u_j''}$, i.e.,

$$\frac{\partial(\bar{\rho}\widetilde{Y_k'' u_j''})}{\partial t} + \frac{\partial(\bar{\rho}\tilde{u}_i \widetilde{Y_k'' u_j''})}{\partial x_i} = \overline{Y_k'' \frac{\partial}{\partial x_i}(\tau_{ij} - \delta_{ij} P)} + \overline{u_j'' \frac{\partial}{\partial x_i}\left(\rho D \frac{\partial Y_k}{\partial x_i}\right)} - \bar{\rho} \widetilde{u_i'' u_j''} \frac{\partial \tilde{Y}_k}{\partial x_i} - \bar{\rho} \widetilde{Y_k'' u_j''} \frac{\partial \tilde{u}_j}{\partial x_i} - \frac{\partial}{\partial x_i}(\overline{\rho Y_k'' u_i'' u_j''}) + \overline{u_j'' \dot{w}_k} \tag{4}$$

one finds the chemistry to directly effect this quantity through the correlation

$$\overline{u_j'' \dot{w}_k} \approx \overline{u_j' \dot{w}_k} = \overline{u_j' \dot{w}_k'} \tag{5}$$

Thus, hoping a simple gradient diffusion type approximation will adequately reproduce the effects of the above term is probably not very realistic. As a result, one expects that the modeling of turbulent diffusion will require different expressions in the absence and presence of combustion. This issue was discussed by Borghi and Dutoya[5] in the context of premixed flames. They assumed a joint Gaussian PDF to model the term indicated in Eq. (5). Such an assumption is not adopted here. Instead an approximate procedure is introduced to model this term.

## Problem Formulation

### Two-Equation Turbulence Model

The two-equation model is based on a turbulent kinetic energy $k$ equation and a turbulent frequency $\omega$ equation, which model a turbulent velocity scale and a turbulent time scale, respectively. The $k$ equation employed in this work has the modeled form

$$\frac{\partial(\bar{\rho}\tilde{k})}{\partial t} + \frac{\partial(\bar{\rho}\tilde{u}_j \tilde{k})}{\partial x_j} = \frac{\partial}{\partial x_j}\left[\left(\mu + \frac{\mu_t}{\sigma_k}\right)\frac{\partial \tilde{k}}{\partial x_j}\right] - \frac{\mu_t}{\bar{\rho}^2}\frac{\partial \bar{\rho}}{\partial x_i}\frac{\partial \bar{P}}{\partial x_i} - C_{k_1}\bar{\rho}\widetilde{u_i'' u_j''}\frac{\partial \tilde{u}_i}{\partial x_j} - C_{k_2}\frac{\bar{\rho}\tilde{k}}{\tau} \tag{6}$$

and similarly the modeled $\omega$ equation can be written as

$$\frac{\partial(\bar{\rho}\tilde{\omega})}{\partial t} + \frac{\partial(\bar{\rho}\tilde{u}_j \tilde{\omega})}{\partial x_j} = \frac{\partial}{\partial x_j}\left[\left(\mu + \frac{\mu_t}{\sigma_\omega}\right)\frac{\partial \tilde{\omega}}{\partial x_j}\right] - C_{\omega_1}\frac{\tilde{\omega}}{\tilde{k}}\bar{\rho}\widetilde{u_i'' u_j''}\frac{\partial \tilde{u}_i}{\partial x_j} - C_{\omega_2}\frac{\bar{\rho}\tilde{\omega}}{\tau} \tag{7}$$

Here, the Reynolds stress is defined as

$$\bar{\rho}\widetilde{u_i'' u_j''} = \frac{2}{3}\delta_{ij}\left(\bar{\rho}\tilde{k} + \mu_t \frac{\partial \tilde{u}_n}{\partial x_n}\right) - \mu_t\left(\frac{\partial \tilde{u}_i}{\partial x_j} + \frac{\partial \tilde{u}_j}{\partial x_i}\right) \tag{8}$$

The one- and two-equation turbulence models differ in their definition of eddy viscosity and turbulent time scale, which are defined as

$$\mu_t = \begin{cases} C_\mu \bar{\rho}\sqrt{\tilde{k}}\, l & \text{one-equation model} \\ C_\mu \bar{\rho}(\tilde{k}/\tilde{\omega}) & \text{two-equation model} \end{cases} \tag{9}$$

$$\tau = \begin{cases} (l/\sqrt{\tilde{k}}) & \text{one-equation model} \\ (1/\tilde{\omega}) & \text{two-equation model} \end{cases} \tag{10}$$

where $l$ is an algebraic expression[6] for the turbulent length scale representative of the width of the mixing layer.

**Table 1 Burner exit conditions**

| Exit conditions | Inner jet | Outer jet | Ambient air |
|---|---|---|---|
| Mach number | 1.0 | 2.0 | 0.0 |
| Temperature, K | 545.0 | 1250.00 | 300.0 |
| Pressure, MPa | 0.112 | 0.107 | 0.101 |
| Mass fraction | | | |
| $Y_{H_0}$ | 1.0 | 0.0 | 0.0 |
| $Y_{O_2}$ | 0.0 | 0.245 | 0.233 |
| $Y_{N_2}$ | 0.0 | 0.580 | 0.757 |
| $Y_{H_2O}$ | 0.0 | 0.175 | 0.01 |
| All others | 0.0 | 0.0 | 0.0 |

Inner jet diameter = 0.002362 m.
Lip thickness = 0.0007239 m.
Outer jet diameter = 0.01778 m.

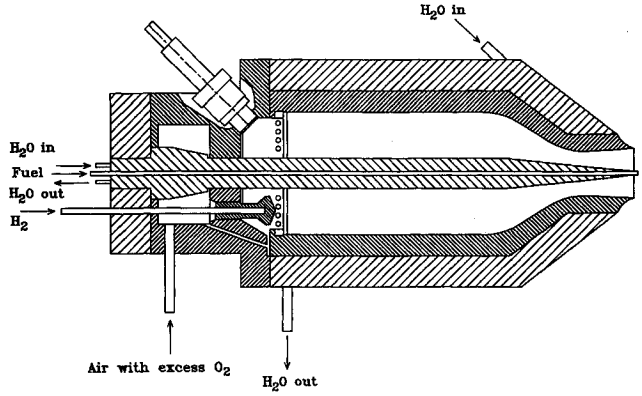


**Fig. 1 Schematic of test apparatus.**

**Table 2 Chemistry model**

| Reaction | $A$ | $b$ | $T_a$ |
|---|---|---|---|
| $H_2 + O_2 \rightleftharpoons OH + OH$ | 1.70E+13 | 0.0 | 24,157.0 |
| $H + O_2 \rightleftharpoons OH + O$ | 1.20E+17 | −0.91 | 8,310.5 |
| $OH + H_2 \rightleftharpoons H_2O + H$ | 2.20E+13 | 0.0 | 2,591.8 |
| $O + H_2 \rightleftharpoons OH + H$ | 5.06E+04 | 2.67 | 3,165.6 |
| $OH + OH \rightleftharpoons H_2O + O$ | 6.30E+12 | 0.0 | 548.6 |
| $HO_2 + H \rightleftharpoons H_2 + O_2$ | 1.30E+13 | 0.0 | 0.0 |
| $HO_2 + H \rightleftharpoons OH + OH$ | 1.50E+14 | 0.0 | 503.3 |
| $HO_2 + O \rightleftharpoons O_2 + OH$ | 2.00E+13 | 0.0 | 0.0 |
| $HO_2 + OH \rightleftharpoons H_2O + O_2$ | 2.00E+13 | 0.0 | 0.0 |
| $HO_2 + H_2 \rightleftharpoons H_2O_2 + H$ | 3.01E+11 | 0.0 | 9,411.2 |
| $HO_2 + HO_2 \rightleftharpoons H_2O_2 + O_2$ | 2.00E+12 | 0.0 | 0.0 |
| $H + H_2O_2 \rightleftharpoons H_2O + OH$ | 1.00E+13 | 0.0 | 1,801.7 |
| $O + H_2O_2 \rightleftharpoons HO_2 + OH$ | 2.80E+13 | 0.0 | 3,220.9 |
| $OH + H_2O_2 \rightleftharpoons H_2O + HO_2$ | 7.00E+12 | 0.0 | 722.2 |
| $H + OH + M \rightleftharpoons H_2O + M$ | 2.21E+12 | −2.0 | 0.0 |
| $H + H + M \rightleftharpoons H_2 + M$ | 7.30E+17 | −1.0 | 0.0 |
| $H + O_2 + M \rightleftharpoons HO_2 + M$ | 2.30E+18 | −1.0 | 0.0 |
| $H_2O_2 + M \rightleftharpoons OH + OH + M$ | 1.21E+17 | 0.0 | 22,898.8 |

Units of $A$ are a multiple of (cm³/mole·s).

**Table 3 Model constants**

| Constants | One-equation model | Two-equation model |
|---|---|---|
| $C_\mu$ | 0.21 | 0.09 |
| $\sigma_k$ | 100/85 | 100/85 |
| $C_{k_1}$ | 1.0 | 1.0 |
| $C_{k_2}$ | 0.13 | 1.0 |
| $\sigma_\omega$ | —— | 100/70 |
| $C_{\omega_1}$ | —— | 0.8 |
| $C_{\omega_2}$ | —— | 1.2 |

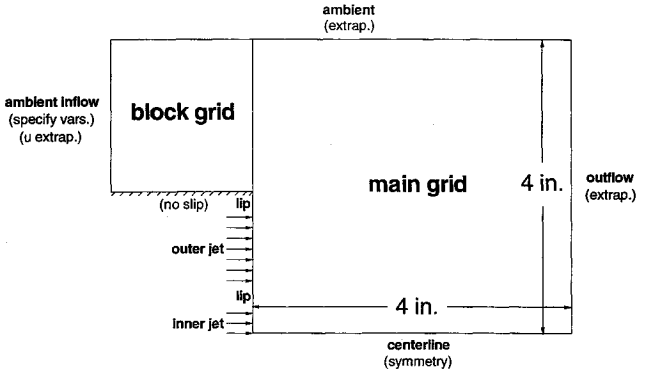


**Fig. 2 Computational domain.**

### Chemical Closure

Since species production rates are nonlinear functions of both temperature and composition, their time averaging requires the implementation of a joint PDF. The averaging is thus

$$\tilde{w}_k = \int \dot{w}_k \mathcal{P}(T, Y_1, \ldots, Y_{ns})\, dT\, dY_1, \ldots, dY_{nx} \quad (11)$$

The joint PDF is assumed to have the form

$$\mathcal{P}(T, Y_1, \ldots, Y_{ns}) = \mathcal{P}(T)\mathcal{P}(Y_1, \ldots, Y_{ns}) \quad (12)$$

Here, $\mathcal{P}(T)$ was chosen as a Gaussian distribution

$$\mathcal{P}(T) = (1/\sqrt{2\pi\overline{T''^2}})\exp\{-[(T - \tilde{T})^2/2\overline{T''^2}]\} \quad (13)$$

and $\mathcal{P}(Y_1, \ldots, Y_{ns})$ was chosen as the multivariate $\beta$ PDF developed by Girimaji,[1] i.e.,

$$\mathcal{P}(Y_1, \ldots, Y_{ns}) = \frac{1}{C}\left[\delta\left(1 - \sum_{k=1}^{ns} Y_k\right)\prod_{k=1}^{ns} Y_k^{\beta_k - 1}\right] \quad (14)$$

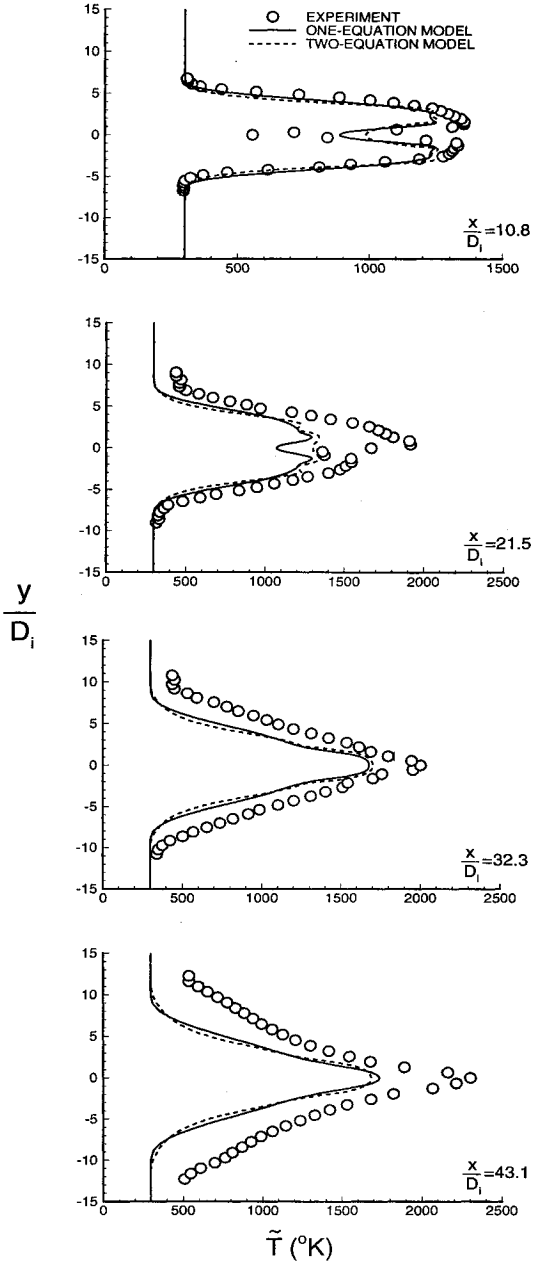


**Fig. 3 Comparison of mean temperature profiles between turbulence models.**

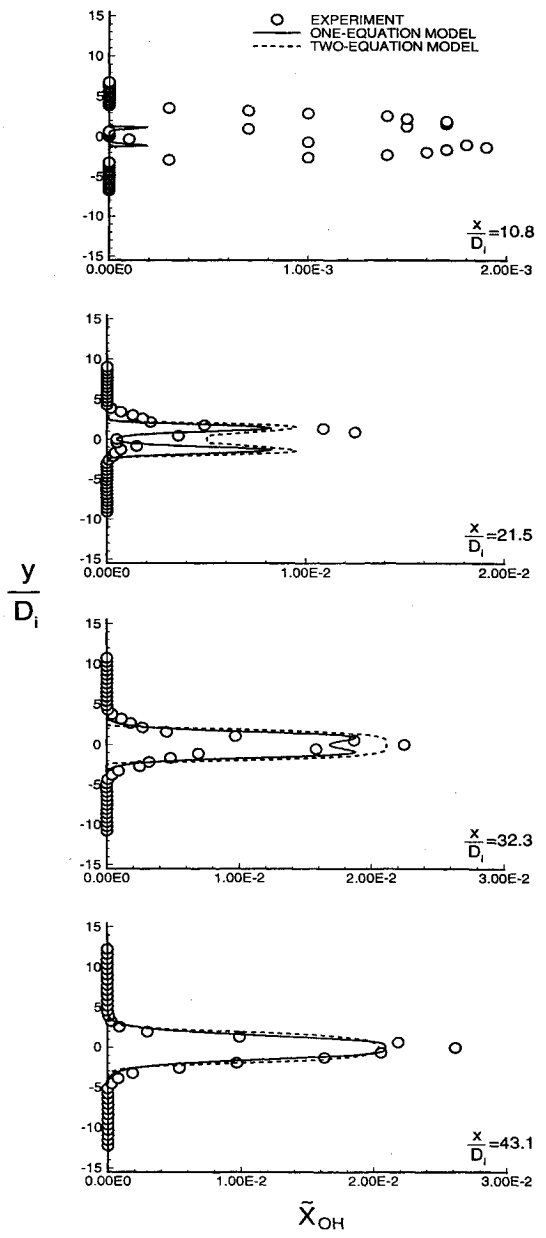


Fig. 4 Comparison of mean OH mole fraction profiles between turbulence models.

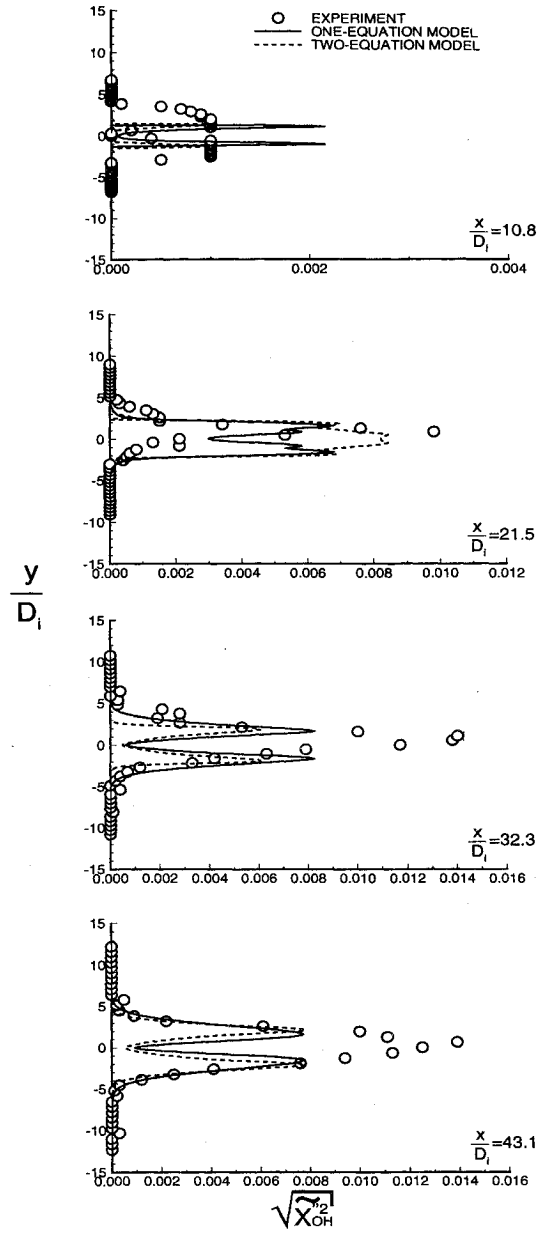


Fig. 5 Comparison of rms mole fraction profiles of the fluctuating component of OH between turbulence models.

It can be shown that[1]

$$C = \left[\prod_{k=1}^{ns} \Gamma(\beta_k) \Big/ \Gamma\left(\sum_{k=1}^{ns} \beta_k\right)\right] \qquad (15)$$
$$\beta_k = \tilde{Y}_k\{[(1 - S)/\tilde{\sigma}_Y] - 1\}$$

where

$$S = \sum_{k=1}^{ns} \tilde{Y}_k^2, \qquad \tilde{\sigma}_Y = \sum_{k=1}^{ns} \widetilde{Y_k'^2} \qquad (16)$$

The governing equation for $\tilde{\sigma}_Y$ is detailed in Refs. 2 and 3 and can be written as

$$\frac{\partial(\bar{\rho}\tilde{\sigma}_Y)}{\partial t} + \frac{\partial(\bar{\rho}\tilde{u}_j\tilde{\sigma}_Y)}{\partial x_j} = \frac{\partial}{\partial x_j}\left(\bar{\rho}D\frac{\partial\tilde{\sigma}_Y}{\partial x_j} - \sum_{k=1}^{ns}\bar{\rho}\widetilde{u_j''Y_k''^2}\right)$$
$$+ 2\sum_{k=1}^{ns}\left(-\bar{\rho}\widetilde{u_j''Y_k''}\frac{\partial\tilde{Y}_k}{\partial x_j} - \bar{\rho}D\overline{\frac{\partial Y_k''}{\partial x_j}\frac{\partial Y_k''}{\partial x_j}} + \overline{\dot{w}_k Y_k''}\right) \qquad (17)$$

where the turbulent terms are modeled as

$$-\sum_{k=1}^{ns}\bar{\rho}\widetilde{u_j''Y_k''^2} = \bar{\rho}D_t\frac{\partial\tilde{\sigma}_Y}{\partial x_j} \qquad (18a)$$

$$-\bar{\rho}\widetilde{u_j''Y_k''} = \bar{\rho}D_t\frac{\partial\tilde{Y}_k}{\partial x_j} \qquad (18b)$$

$$\sum_{k=1}^{ns}\bar{\rho}D\overline{\frac{\partial Y_k''}{\partial x_j}\frac{\partial Y_k''}{\partial x_j}} = C_{\sigma_Y}\frac{\bar{\rho}\tilde{\sigma}_Y}{2\tau} \qquad (18c)$$

The PDFs have nonzero values only in the realizable domain. If the inlet flow is not turbulent, then the minimum temperature needed to clip the Gaussian distribution would be the inlet temperature. However, in this work, the inlet flows are turbulent. Thus, the distribution was clipped based on the following temperature range:

$$T_{\min} = \min(\tilde{T} - n_1\sqrt{\widetilde{T''^2}}, 300) \qquad (19)$$
$$T_{\max} = \max(\tilde{T} + n_1\sqrt{\widetilde{T''^2}}, 3000)$$

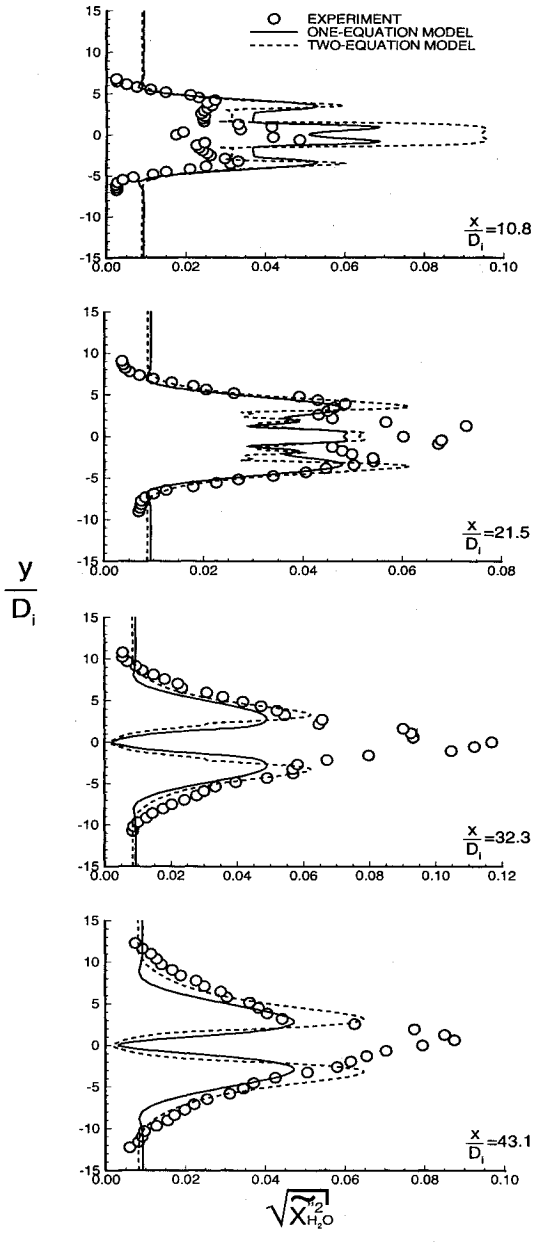


Fig. 6 Comparison of rms mole fraction profiles of the fluctuating component of $H_2O$ between turbulence models.

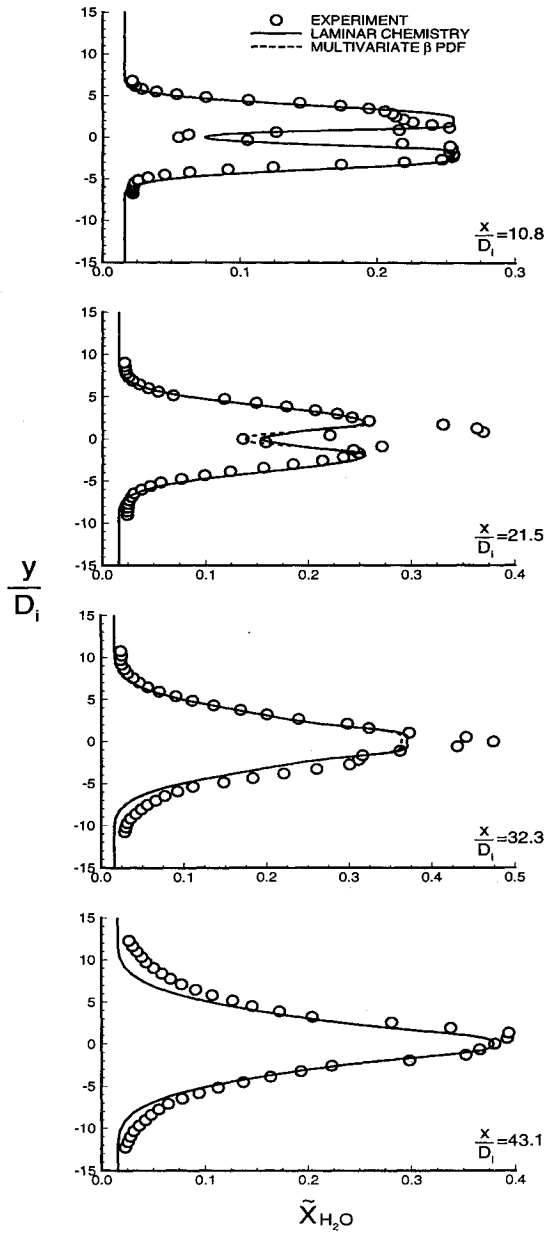


Fig. 7 Comparison of mean $H_2O$ mole fraction profiles with and without the PDF.

where 300 and 3000 represent the temperature range (in Kelvin) for which the Arrhenius expressions are valid, and $n_1$ is a scaling factor that ensures the clipped portions of the distribution are small enough such that the PDF approximately integrates to unity. A value of 5 for this factor was found to be an adequate choice. A detailed parametric study of the temperature PDF is described in Ref. 7.

For the multivariate $\beta$ distribution to be defined, each $\beta_k$ must be nonnegative. This realizability condition is met if

$$[(1 - S)/\bar{\sigma}_Y] - 1 \geq 0 \tag{20}$$

which reduces to the physical constraint

$$\sum_{k=1}^{ns} \overline{Y_k''^2} \leq 1 \tag{21}$$

A detailed parametric study of the multivariate $\beta$ PDF is described in Ref. 8.

The Favre-averaged Navier-Stokes equations together with the species conservation equations, transport properties, and chemistry model are described in Ref. 9. The equation governing the temperature (or enthalpy) variance is described in Refs. 6 and 10.

### Proposed PDF for Favre Averaging

The Favre-averaged mass fractions are related to the time-averaged species densities through the relation

$$\bar{\rho}_k = \bar{\rho}\tilde{Y}_k \tag{22}$$

Thus, in order to calculate $\tilde{Y}_k$, a joint PDF of the species densities is required. This function is given by the following multivariate $\beta$ distribution:

$$\mathcal{P}(\rho_1^*, \ldots, \rho_{ns}^*) = \frac{1}{C^*}(1 - \rho^*)^{(\alpha-1)} \times \prod_{k=1}^{ns} \rho_k^{*(\beta_k^*-1)} \delta\left(\rho^* - \sum_{k=1}^{ns} \rho_k^*\right) \tag{23}$$

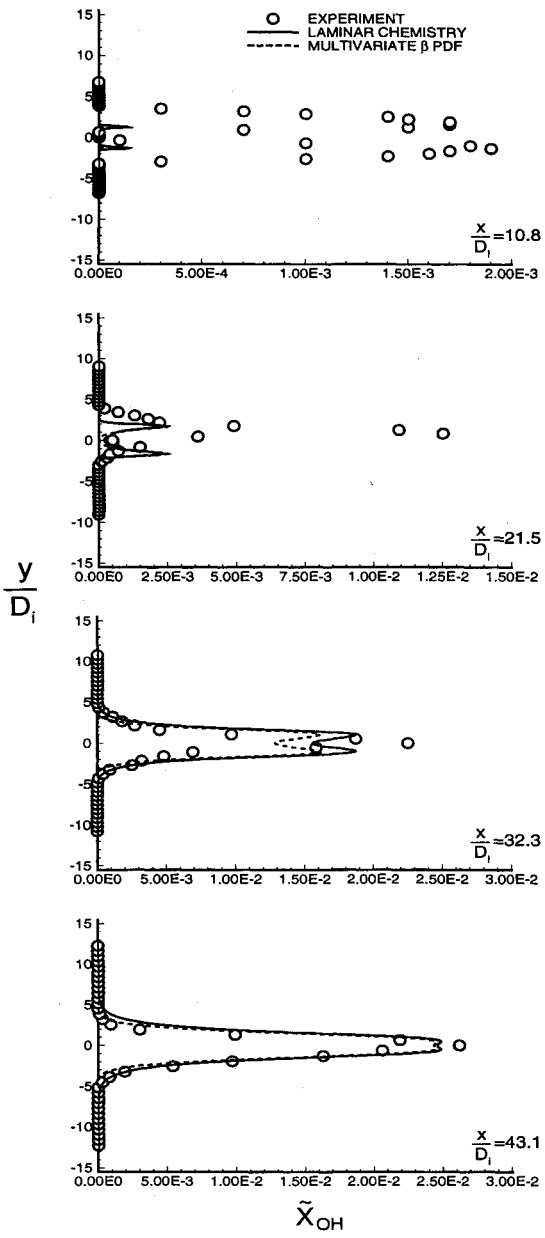


Fig. 8 Comparison of mean OH mole fraction profiles with and without the PDF.

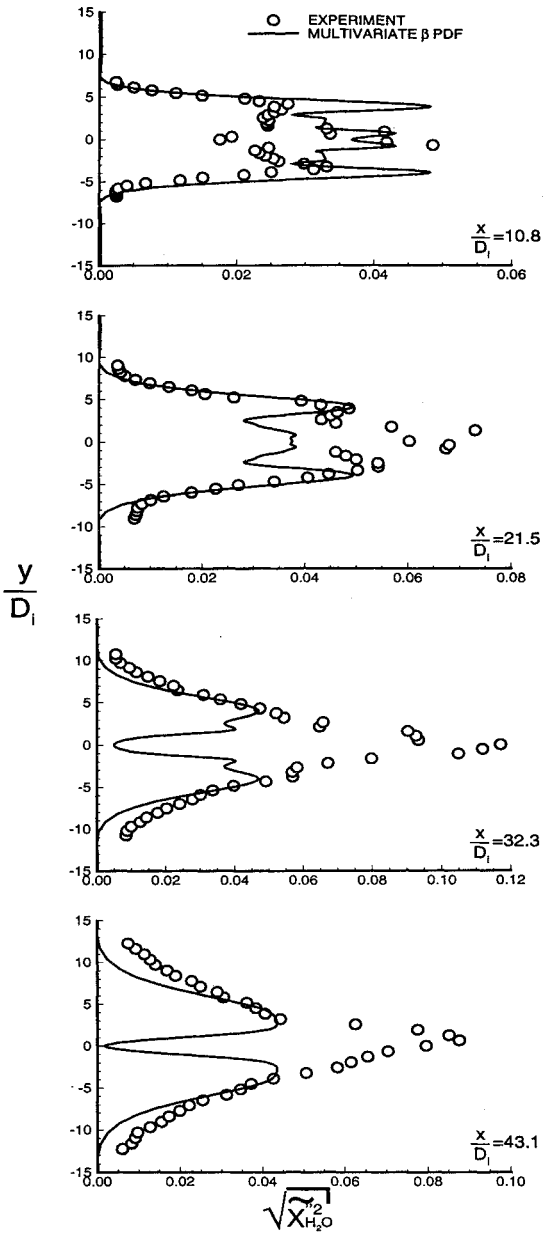


Fig. 9 Comparison of rms mole fraction profiles of the fluctuating component of $H_2O$ with experiment.

where

$$C^* = \frac{\Gamma(\alpha)}{\Gamma(\gamma)} \sum_{k=1}^{ns} \Gamma(\beta_k^*)$$
$$\gamma = \alpha + \sum_{k=1}^{ns} \beta_k^*, \qquad \rho_k^* = \frac{\rho_k}{\rho_{\max}} \tag{24}$$

In the above, $\rho_{\max}$ represents the maximum instantaneous density.

The unknowns $\beta_k^*$ and $\alpha$ can be determined knowing only the mean species densities and the quantity $\tilde{\sigma}_\rho \equiv \Sigma_{k=1}^{ns} \overline{\rho_k'^2}$ through the relationship

$$\gamma = \left[ \left( \bar{\rho}\rho_{\max} - \sum_{k=1}^{ns} \bar{\rho}_k^2 \right) \Big/ \tilde{\sigma}_\rho \right] - 1, \qquad \beta_k^* = \gamma \bar{\rho}_k^* \tag{25}$$

where the quantity $\rho_{\max}$ is approximated by

$$\rho_{\max} = \bar{\rho} + n_2 \sqrt{\tilde{\sigma}_\rho} \tag{26}$$

and $n_2$ is a scaling factor. The solution was found to be insensitive to the precise value of $n_2$, however, this value must be large enough to ensure that $\gamma$ is nonnegative. A value of 10 was used in these calculations.

Since the mean species densities are obtained from the Favre-averaged species continuity equations, only one extra transport equation for $\tilde{\sigma}_\rho$ is needed. This equation is derived from the species continuity equations with $\rho_k$ and $u_j$ decomposed as follows:

$$\rho_k = \bar{\rho}_k + \rho_k', \qquad u_j = \tilde{u}_j + u_j'' \tag{27}$$

The resulting equation for $\tilde{\sigma}_\rho$ is then given by

$$\frac{\partial \tilde{\sigma}_\rho}{\partial t} + \frac{\partial (\tilde{\sigma}_\rho \tilde{u}_j)}{\partial x_j} = \frac{\partial}{\partial x_j} \left( D \frac{\partial \tilde{\sigma}_\rho}{\partial x_j} - \sum_{k=1}^{ns} \overline{\rho_k'^2 u_j''} \right) - \tilde{\sigma}_\rho \frac{\partial \tilde{u}_j}{\partial x_j}$$
$$+ 2 \sum_{k=1}^{ns} \left( -\overline{\rho_k' u_j''} \frac{\partial \bar{\rho}_k}{\partial x_j} - D \overline{\frac{\partial \rho_k'}{\partial x_j} \frac{\partial \rho_k'}{\partial x_j}} + \overline{\rho_k' \dot{w}_k} \right) \tag{28}$$

where the terms

$$2\left(\bar{\rho}_k\overline{u_j''\frac{\partial\rho_k'}{\partial x_j}} - \bar{\rho}_k\frac{\partial(\overline{\rho_k'u_j''})}{\partial x_j}\right), \quad \left(\overline{u_j''\frac{\partial\rho_k'^2}{\partial x_j}} - \frac{\partial(\overline{\rho_k'^2u_j''})}{\partial x_j}\right) \tag{29}$$

have been neglected. These terms have been dropped because once modeled, they represent differences in second derivatives that are zero if

$$\frac{\partial}{\partial x_j}\left(D_t\frac{\partial\overline{\rho_k'^2}}{\partial x_j}\right) \approx D_t\frac{\partial^2\overline{\rho_k'^2}}{\partial x_j\partial x_j}$$
$$\bar{\rho}_k\frac{\partial}{\partial x_j}\left(D_t\frac{\partial\bar{\rho}_k}{\partial x_j}\right) \approx \bar{\rho}_kD_t\frac{\partial^2\bar{\rho}_k}{\partial x_j\partial x_j} \tag{30}$$

The unclosed moments are modeled with the traditional gradient diffusion approximation as follows:

$$\sum_{k=1}^{ns}\overline{\rho_k'^2u_j''} = -D_t\frac{\partial\bar{\sigma}_\rho}{\partial x_j} \tag{31a}$$

$$\overline{\rho_k'u_j''} = -\bar{\rho}D_t\frac{\partial\tilde{Y}_k}{\partial x_j} \tag{31b}$$

$$\sum_{k=1}^{ns}D\overline{\frac{\partial\rho_k'}{\partial x_j}\frac{\partial\rho_k'}{\partial x_j}} = C_{\sigma_\rho}\frac{\bar{\sigma}_\rho}{2\tau} \tag{31c}$$

where $C_{\sigma_\rho}$ was chosen as one-half. The chemical source term $\sum_{k=1}^{ns}\rho_k'\dot{w}_k$ is calculated directly from the assumed PDF by noting that

$$\sum_{k=1}^{ns}\overline{\rho_k'\dot{w}_k} = \sum_{k=1}^{ns}\overline{\rho_k\dot{w}_k} - \sum_{k=1}^{ns}\bar{\rho}_k\tilde{\dot{w}}_k \tag{32}$$

**Countergradient Diffusion Model**

As shown below, use of the above PDF did not improve agreements with experiment. Therefore, since it is more convenient to work with the mass fractions rather than the species densities, the multivariate $\beta$ PDF proposed by Girimaji was employed. It is proposed that, in the presence of reactions, the turbulent mass diffusion be modeled as

$$\bar{\rho}\widetilde{Y_k''u_j''} = -\bar{\rho}D_t\frac{\partial\tilde{Y}_k}{\partial x_j} - C_w\frac{\bar{\rho}D_t}{\bar{P}}\overline{u_j''\dot{w}_k'} \tag{33}$$

Proper modeling of $\overline{u_j''\dot{w}_k'}$ requires the use of a joint velocity-scalar PDF. In the absence of such an expression, a different approach will be employed.

The term of interest in the variance equation is the production term $\bar{\rho}\widetilde{Y_k''u_j''}(\partial\tilde{Y}_k/\partial x_j)$, so rather than modeling $\overline{u_j''\dot{w}_k'}$, the term $\overline{u_j''\dot{w}_k'}(\partial\tilde{Y}_k/\partial x_j)$ will be modeled. Starting with the species conservation equation governing $\bar{\rho}Y_k''$ and neglecting higher order quantities one obtains

$$\frac{\partial}{\partial x_j}(\bar{\rho}\tilde{u}_jY_k'' + \bar{\rho}\tilde{Y}_ku_j'') \approx \dot{w}_k' \tag{34}$$

or, ignoring the spatial derivatives of the fluctuating quantities, the above expression reduces to

$$u_j''\frac{\partial}{\partial x_j}(\bar{\rho}\tilde{Y}_k) \approx \dot{w}_k' \tag{35}$$

For the purpose of modeling, the above term is approximated by

$$\bar{\rho}u_j''\frac{\partial\tilde{Y}_k}{\partial x_j} \approx \dot{w}_k' \tag{36}$$

Multiplying both sides by $\dot{w}_k'$ and averaging then yields

$$\bar{\rho}\overline{u_j''\dot{w}_k'}\frac{\partial\tilde{Y}_k}{\partial x_j} \approx \overline{\dot{w}_k'^2} = \overline{\dot{w}_k^2} - \dot{w}_k^2 \tag{37}$$

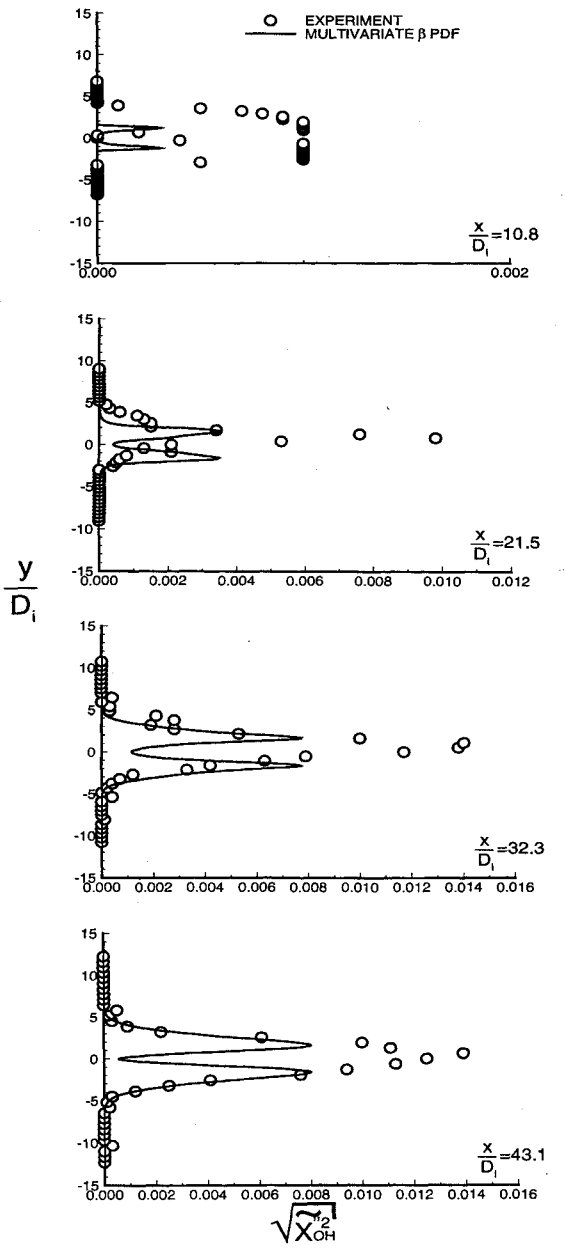


**Fig. 10 Comparison of rms mole fraction profiles of the fluctuating component of OH with experiment.**

The quantity $\overline{\dot{w}_k^2}$ can be calculated directly from the assumed PDF.

## Results and Discussion

A schematic of the supersonic burner is given in Fig. 1, and the burner exit conditions are summarized in Table 1. The chemistry model employed is the 18-step model of Jachimowski[11] shown in Table 2 where the constants describe the Arrhenius expression for the forward reaction rate, $k_f(T) = AT^b\exp(-T_a/T)$. All calculations were carried out using a 93 × 93 grid on a domain of 4 × 4 in. (≈43 i.d.) with a 37 × 29 block added to the ambient inflow boundary. A schematic of the computational setup is given in Fig. 2.

All calculations were carried out using a cell-centered finite volume code developed at North Carolina State University. The numerical scheme used is described in Ref. 9. The base calculations required approximately 2 h of Cray time using the 18-step kinetic model, and the increase in CPU time when the PDFs are employed was approximately 25%.

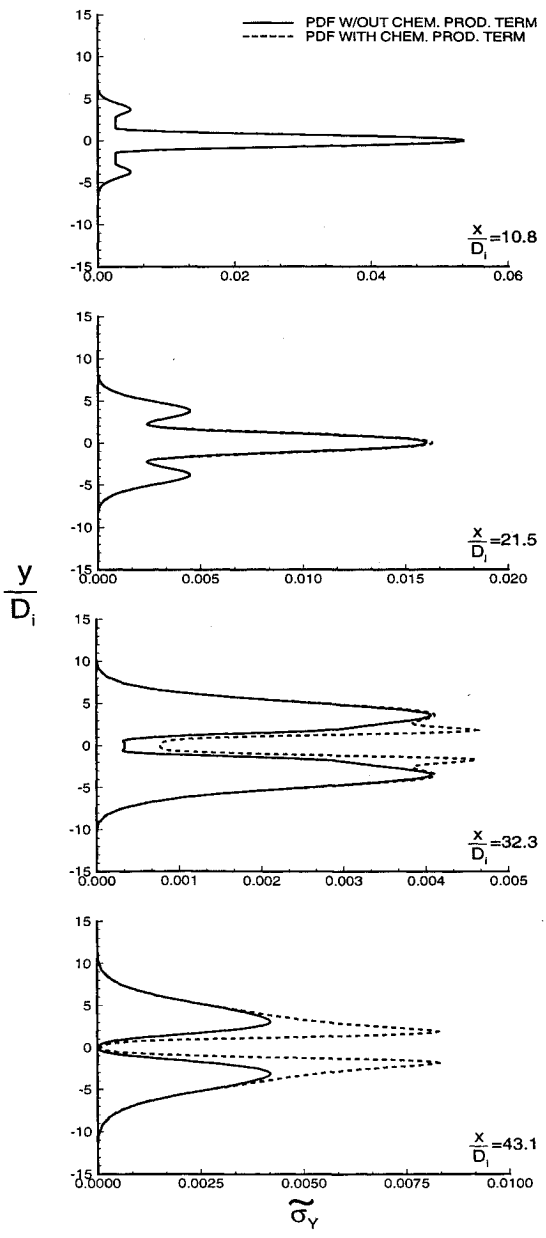


Fig. 11 Comparison of $\tilde{\sigma}_Y$ profiles with and without the chemical production term.

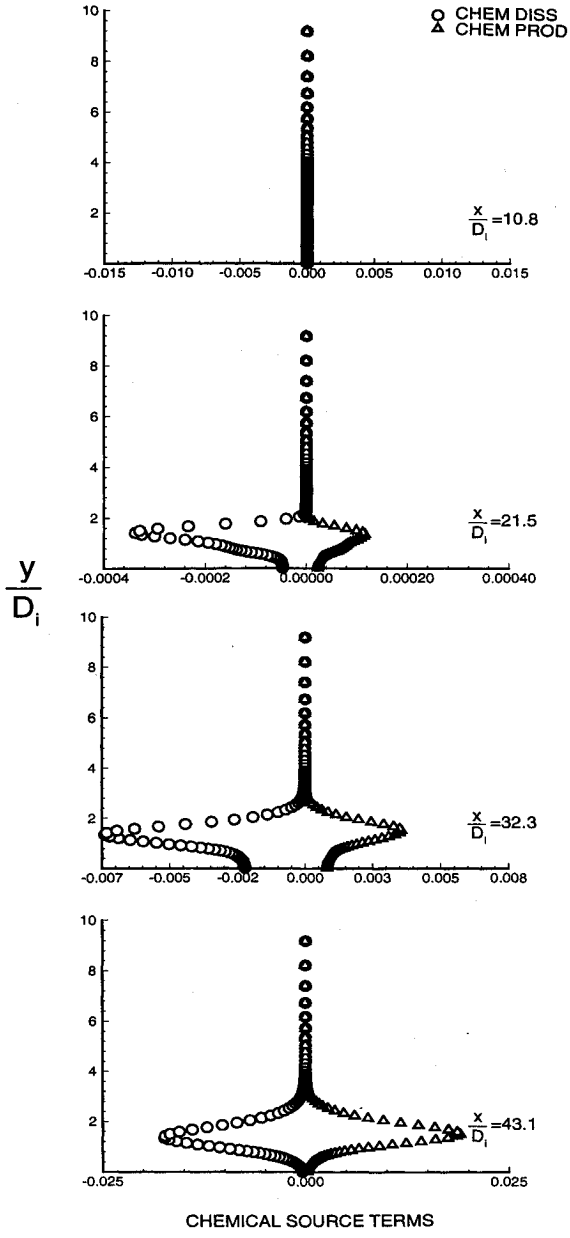


Fig. 12 Comparison of chemical source terms in the equation governing $\tilde{\sigma}_Y$.

The role of the turbulence model employed is considered first. The boundary conditions for the TKE were chosen as $(\sqrt{\tilde{k}}/|\tilde{u}_j|) = 1\%$ for both streams. The $\tilde{\omega}$ boundary conditions in these regions were set to $(\sqrt{\tilde{k}}/l_i)$, where $l_i$ represents the initial mixing length with a value in the range of the inner-outer jet lip height. All walls were treated as adiabatic and noncatalytic, and all other boundary conditions are outlined in Fig. 2. The model constants for the two models used in this investigation are provided in Table 3, and the constant $C_{\sigma_Y}$ was chosen as one-fourth. The $k$-$\omega$ model constants were obtained by Anderson,[12] who developed a model to calculate turbulent flows over bodies and their wakes for both low- and high-speed flows. This model was used because, to our knowledge, it is the only model that gives the correct growth rate of the wake behind a flat plate at zero angle of attack.

All results compare calculations to the experimental measurements of Ref. 4 at downstream locations of 10.8, 21.5, 32.3, and 43.1 inner jet diameters (or 1, 2, 3, and 4 in.). Due to space limitations, only a small fraction of the results will be presented. Further details are available in Refs. 13 and 14. The results of a sensitivity analysis of the solution to grid refinement, boundary condition specification, and inlet turbulent intensities can be found in Ref. 15. Figure 3 compares the mean temperature, and Fig. 4 compares the mean OH mole fraction with experiment. As seen from the figures, both models show good agreement with each other. As a result, the two-equation model failed to better predict the shear layer growth downstream of the burner. Figures 5 and 6 compare the rms of the fluctuations of OH and $H_2O$. The two-equation model shows better predictions near the centerline for the first two stations. However, after ignition, both models severely underpredict the variance near the centerline. Hence, the form of the turbulence model used is not the cause of the reduced variance in the combustion zone.

Because the two-equation turbulence model had little influence on the results, the remaining calculations employed the one-equation turbulence model. Moreover, in order to isolate the influence of species mass fractions, the PDF for the next set of calculations has the form

$$\mathcal{P}(T, \rho_k) = \delta(T - \tilde{T})\mathcal{P}(\rho_k^*) \tag{38}$$

Figures 7 and 8 show that the effect of the PDF is minimal on the mean $H_2O$ and OH mole fractions. The small impact

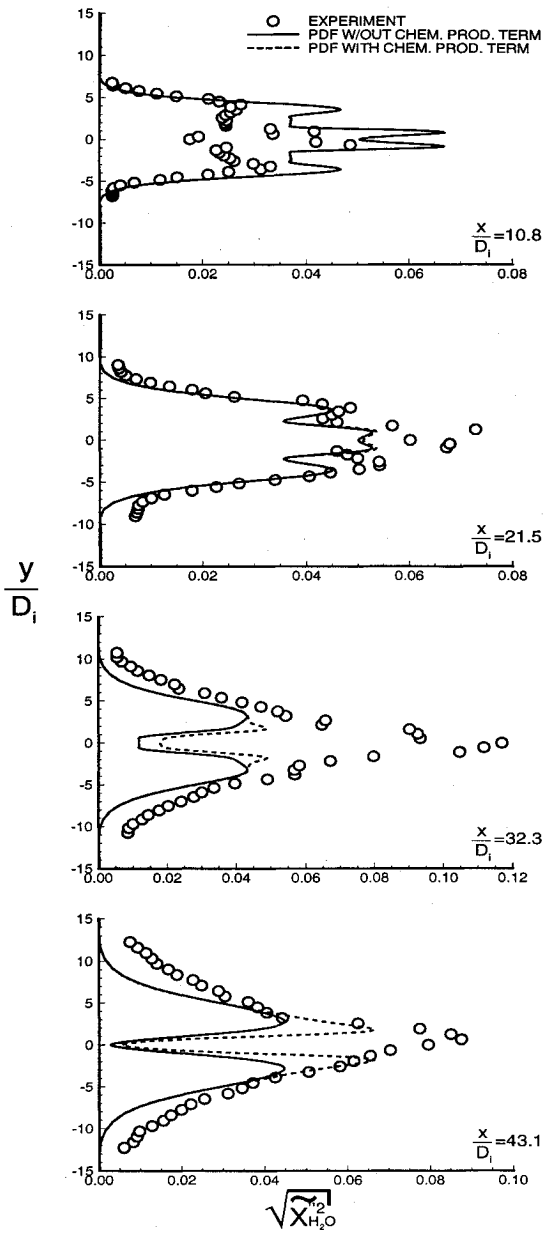


**Fig. 13 Comparison of rms mole fraction profiles of the fluctuating component of $H_2O$ with and without the chemical production term.**

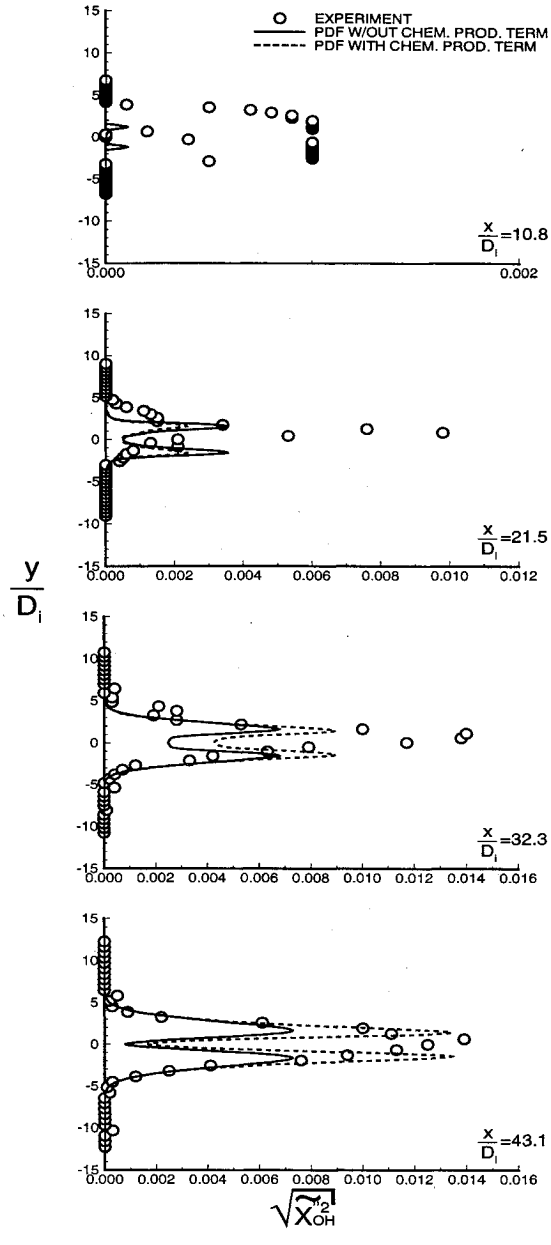


**Fig. 14 Comparison of rms mole fraction profiles of the fluctuating component of OH with and without the chemical production term.**

was such that it resulted in a slight delay in the onset of combustion. It is difficult to assess exactly why the PDF delayed the combustion process. A possible explanation follows from the forms of the multivariate $\beta$ PDFs employed and the reactions employed. The averages of the forward rates that result in the initial formation of the radicals O, H, and OH (see the first 4 reactions in Table 2) lead to covariances. The PDFs employed yield covariances that are always negative. This will have the effect of reducing the effective production rates of the radicals. There is no reason to expect that such behavior is representative of $H_2$-air flames.

Figures 9 and 10 show the mole fraction rms of the fluctuating components for $H_2O$ and OH. These figures show good agreement in the regions preceding combustion, but large discrepancies are noted at the 3- and 4-in. stations in the presence of combustion due to small values of $\tilde{\sigma}_\rho$. The depletion of the density variance sum in the regions of combustion was due primarily to the chemical source term $\Sigma_{k=1}^{ns} \rho_k' \dot{w}_k$ which, as mentioned previously, acts as a strong dissipation term. Since this same behavior was evident in the PDF model of Girimaji, it is possible the discrepancy may not be due to the form of the PDF, but rather to the modeling of the transport equation governing the species variance sum. As a result, our attention will be directed to the terms resulting from the inclusion of the countergradient diffusion.

Figure 11 shows the effect of incorporating the countergradient diffusion term (with $C_w = 0.4$) into the equation governing the species mass fraction variance sum ($\tilde{\sigma}_Y$). Since the goal of this exercise is to examine the effect of the above term, an abridged version of the reaction set that neglected the species $H_2O_2$ and $HO_2$ was used. As can be seen, the added chemical production term did increase the species variance sum, but unfortunately did little to improve the results at the centerline. Thus, further refinement of the modeling is needed. Figure 12 compares the size of the modeled chemical production term relative to the chemical dissipation term. In this figure, the circles represent the chemical dissipation term, and the triangles represent the chemical production term. This figure shows the chemical dissipation term to be about twice that of the chemical production term at the 3-in. station, and a balance is eventually achieved between the 3- and 4-in. stations.

Figures 13 and 14 compare the computed rms of the fluctuations of $H_2O$ and OH with and without the use of the

modeled chemical production term. They show improvements when the chemical production term is added.

## Concluding Remarks

Based on present calculations, differences resulting from the two turbulence models employed and differences between Favre and time averaging the species mass fractions did not account for the large dissipative nature of the chemical source term appearing in the transport equation for the species variance sum. Although the multivariate $\beta$ PDF models employed result in covariances that are always negative, we cannot ascertain at this time that the discrepancy is solely a direct result of the PDF employed. This has to await the results of a modeled PDF, direct numerical simulation, or some other joint PDF that does not exhibit similar behavior. Based on present results, we believe that another possible cause lies in the modeling of the turbulent diffusion. Simple gradient diffusion approximations that may be well-suited for nonreacting flows are not capable of accounting for the effects of the reactions. The simple proposal made here for modeling the countergradient diffusion resulted in modest improvements in the predictions. As a result, a more elaborate model for the countergradient diffusion may help bridge the gap between theory and experiment.

## Acknowledgments

This work is supported in part by the following grants: NASA Grant NAG-1-244 and the Mars Mission Center funded by NASA Grant NAGW-1331.

## References

[1]Girimaji, S. S., "A Simple Recipe for Modeling Reaction-Rates in Flows with Turbulent Combustion," AIAA Paper 91-1792, June 1991.

[2]Narayan, J. R., and Girimaji, S. S., "Turbulent Reacting Flow Computations Including Turbulence-Chemistry Interactions," AIAA Paper 92-0342, Jan. 1992.

[3]Baurle, R. A., Alexopoulous, G. A., Hassan, H. A., and Drummond, J. P., "An Assumed Joint-Beta PDF Approach for Supersonic Turbulent Combustion," AIAA Paper 92-3844, July 1992.

[4]Cheng, T. S., Wehrmeyer, J. A., Pitz, R. W., Jarrett, O., Jr., and Northam, G. B., "Finite-Rate Chemistry Effects in a Mach 2 Reacting Flow," AIAA Paper 91-2320, June 1991.

[5]Borghi, R., and Dutoya, D., "On the Scales of the Fluctuations in Turbulent Combustion," *Proceedings of the 17th Symposium (International) on Combustion*, The Combustion Inst., Pittsburgh, PA, 1978, pp. 235–244.

[6]Baurle, R. A., Drummond, J. P., and Hassan, H. A., "An Assumed PDF Approach for the Calculation of Supersonic Mixing Layers," AIAA Paper 92-0182, Jan. 1992.

[7]Gaffney, R. L., White, J. A., Girimaji, S. S., and Drummond, J. P., "Modeling Turbulent/Chemistry Interactions Using Assumed PDF Methods," AIAA Paper 92-3638, July 1992.

[8]Gaffney, R. L., White, J. A., Girimaji, S. S., and Drummond, J. P., "Modeling Temperature and Species Fluctuations in Turbulent, Reacting Flow," *Journal of Computational Mechanics* (to be published).

[9]Eklund, D. R., Drummond, J. P., and Hassan, H. A., "Numerical Modeling of Turbulent Supersonic Reacting Coaxial Jets," *AIAA Journal*, Vol. 28, No. 9, 1990, pp. 1633–1641.

[10]Frankel, S. H., Drummond, J. P., and Hassan, H. A., "A Hybrid Reynolds Averaged/PDF Closure Model for Supersonic Turbulent Combustion," AIAA Paper 90-1573, June 1990.

[11]Jachimowski, C. J., "An Analytic Study of the Hydrogen-Air Reaction Mechanism with Application to Scramjet Combustion," NASA TP 2791, Feb. 1988.

[12]Anderson, E. C., private communication, NASA Langley Research Center, Hampton, VA.

[13]Alexopoulos, G. A., Baurle, R. A., and Hassan, H. A., "A $k$-$\omega$ Multivariate Beta PDF for Supersonic Turbulent Combustion," AIAA Paper 93-2197, June 1993.

[14]Baurle, R. A., and Hassan, H. A., "Modeling of Turbulent Supersonic $H_2$-Air Combustion with a Multivariate $\beta$ PDF," AIAA Paper 93-2198, June 1993.

[15]Baurle, R. A., Alexopoulos, G. A., and Hassan, H. A., "An Assumed Joint PDF Approach for Supersonic Turbulent Combustion," *Journal of Propulsion and Power*, Vol. 10, No. 4, 1994, pp. 473–484.